Chemical Science

ROYAL SOCIETY OF CHEMISTRY

EDGE ARTICLE

View Article Online
View Journal

Cite this: DOI: 10.1039/d6sc01628f

All publication charges for this article have been paid for by the Royal Society of Chemistry

Non-radical pathways control methane sulfonation *versus* oxygenation C–H functionalization selectivity with Hg(II) and Au(III) catalysis

Anjaneyulu Koppaka,†*[a] Caz Cullimore,†[a] Jyothish Joy,[a] Alex Kraus,[a] Roy A. Periana*[b] and Daniel H. Ess *[a]

Received 25th February 2026
Accepted 10th April 2026

DOI: 10.1039/d6sc01628f

rsc.li/chemical-science

Methane C–H functionalization by radical pathways is often unselective and not desirable. Transition metal catalyzed C–H functionalization of methane to methanesulfonic acid (sulfonation) in sulfuric acid has generally been interpreted as resulting from a radical mechanism whereas functionalization to methyl bisulfate (oxygenation) has been proposed to occur by both radical and non-radical pathways. For Hg^{II} and Au^{III} catalysis, formation of either methanesulfonic acid or methyl bisulfate depends on whether 98% sulfuric acid or oleum (SO_3 added) is used. Here we report new experiments combined with density functional theory calculations that have revealed that selectivity is determined by non-radical pathways where a Hg^{II}/Au^{III}-methyl intermediate can undergo either an electrophilic substitution pathway (S_E2) with SO_3 to form methanesulfonic acid or a nucleophilic substitution pathway (S_N2) with bisulfate to form methyl bisulfate. The favored pathway is determined by the electrophilicity/reduction potential of the metal and the sulfuric acid to SO_3/H_2O equilibrium. Overall, this new selectivity model provides a straightforward understanding of product selectivity and does not require a functionalization mechanism involving radicals.

Introduction

Functionalization of light alkane C–H bonds, especially methane, remains an important and unsolved catalysis challenge.[1–9] There are only a few homogeneous transition metal[10–14] and main group[15–17] systems that have been reported to catalyze or promote direct methane conversion to a C–H functionalized product. The most highly efficient catalysts operate in concentrated sulfuric acid, either in 98% sulfuric acid or in oleum (SO_3-added to sulfuric acid). While sulfuric acid provides a solvent suitable for high reactivity, sulfonation functionalization to methanesulfonic acid (CH_3SO_3H) or oxygenation functionalization to methyl bisulfate (CH_3OSO_3H) depends on the metal center, the exact solvent formulation, and reaction conditions (Fig. 1, Panel A). There is currently no unifying mechanistic model that provides the origin of sulfonation *versus* oxygenation selectivity for different metals and different formulations of sulfuric acid solvent. Also, it has often been proposed that methane C–H functionalization to methanesulfonic acid occurs through a radical reaction pathway where SO_3 captures a methyl radical intermediate (Fig. 1, Panel B).[18–20]

We decided to experimentally and computationally examine and compare Hg^{II} and Au^{III} because these metals give different product selectivity in sulfuric acid, and the selectivity depends on the exact sulfuric acid formulation. Periana reported that $Hg^{II}(SO_4)$ in 98% sulfuric acid, which transforms to $Hg^{II}(HSO_4)_2$, catalyzes conversion of methane to methyl bisulfate (oxygenation) at 180 °C.[21] In contrast to the 98% sulfuric acid conditions, methane reactions conducted by Sen and coworkers with $Hg^{II}(SO_4)$ in oleum at 160 °C resulted in methanesulfonic acid (sulfonation) being the major product and methyl bisulfate as a minor product.[19,20,22] At 90 °C Sen found that only methanesulfonic acid was formed, indicating this is the kinetic product in oleum, and this result and similar results have been generally interpreted as evidence for a radical functionalization mechanism.

For Au^{III}, Au_2O_3 dissolved in 98% sulfuric acid at 180 °C catalyzed conversion of methane to methyl bisulfate.[23] Au^{III} catalysis has never been examined at lower temperatures, such as 90 °C, and so it is unknown whether methanesulfonic acid or methyl bisulfate is the kinetic product. Also, while reactions with Au^0 have been examined in SO_3 added sulfuric acid, there has previously been no report of reactions of Au_2O_3 with methane in significant quantities of SO_3, such as 20% weight in H_2SO_4.

With this experimental background, we decided to complete the low temperature and oleum experiments with Au^{III}. Here we report that at lower temperatures in both 98% sulfuric acid and oleum, Au^{III} led to the exclusive formation of methyl bisulfate.

[a]Department of Chemistry and Biochemistry, Brigham Young University, Provo, UT 84604, USA. E-mail: Anjaneyulu.Koppaka@byu.edu; dhe@byu.edu

[b]The Herbert Wertheim UF Scripps Institute for Biomedical Innovation & Technology, University of Florida, Jupiter, Florida 33458, USA. E-mail: perianar@gmail.com

† Contributed equally.

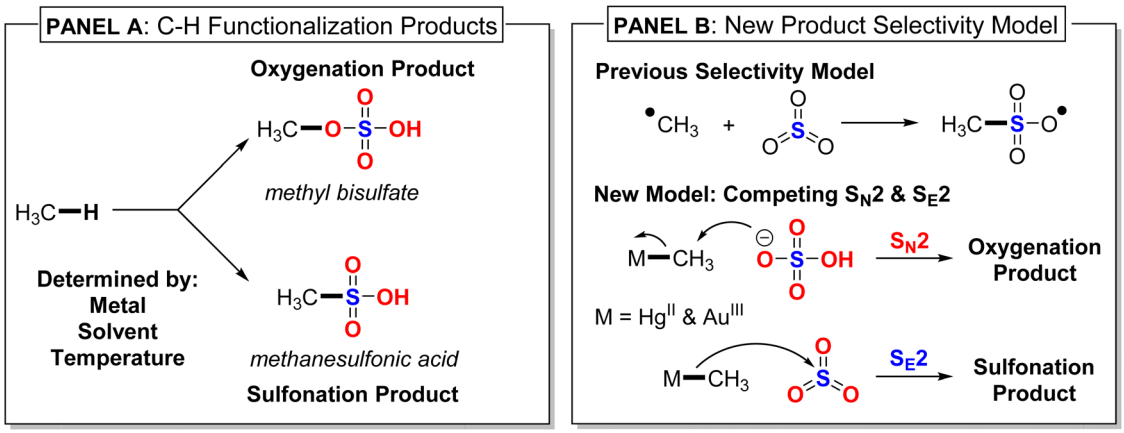

Fig. 1 Panel (A) outline of methane C–H functionalization products, which depends on the metal center, the sulfuric acid solvent formulation (98% or oleum), and reaction temperature. Panel (B) outline of the previously proposed radical pathway leading to methanesulfonic acid and the new selectivity model showing that from the metal–methyl intermediate there is competition between S_N2 and S_E2 functionalization pathways.

Also, new low-temperature experiments with Hg^{II} in 98% sulfuric acid showed only methyl bisulfate as the kinetic product, while in oleum there was no detectable formation of methyl bisulfate. This means that Au^{III} and Hg^{II} have fundamentally different kinetic product selectivity for C–H functionalization. Density functional theory (DFT) calculations were then used to determine the origin of oxygenation *versus* sulfonation selectivity. In contrast to previous proposals where a radical mechanism has been used to rationalize sulfonation selectivity,[18–20] our DFT calculations indicate that selectivity arises from closed-shell reactivity differences between Hg^{II}–CH_3 and Au^{III}–CH_3 intermediates (Fig. 1, Panel B). For Hg^{II}–CH_3, the electrophilic S_E2 substitution transition state with SO_3 is inherently lower in energy than the nucleophilic S_N2 substitution transition state with bisulfate. Therefore, in oleum, methanesulfonic acid is the kinetic product. In contrast, in 98% sulfuric acid, the ground state sulfuric acid to SO_3/H_2O equilibrium disfavors the S_E2 pathway, resulting in a lower energy S_N2 kinetic pathway to methyl bisulfate. For Au^{III}–CH_3, the inherent transition state energies are reversed, and the S_N2 reaction pathway is always lower in energy than the S_E2 pathway, resulting in only methyl bisulfate product formation.

Results and discussion

Overview of previous Hg^{II} and Au^{III} reactions

To maximize reactivity and minimize overoxidation, the most effective homogeneous transition metal and main-group metal methane C–H functionalization catalysts use concentrated sulfuric acid as the solvent, either 98% sulfuric acid or oleum, which has added SO_3. Perhaps the most catalytically efficient system is Hg^{II} in 98% sulfuric acid. Periana and coworkers reported that $Hg^{II}(SO_4)$ catalyzes conversion of methane to methyl bisulfate at 180 °C with a turnover frequency of about 10^{-3} s^{-1} with minimal generation of CO_2 and other over-oxidized products.[21] Experimental measurements by Periana, which included deuterium isotopologue incorporation studies, and more recently our DFT calculations,[24] led to the proposed catalytic cycle outlined in Fig. 2 (Panel A). In this cycle, a non-radical C–H activation/metalation reaction step (also called electrophilic substitution), generates a Hg^{II}–CH_3 intermediate, which upon reductive functionalization gives methyl bisulfate. Similar to Hg^{II}, Au_2O_3 dissolved in 98% sulfuric acid at 180 °C converts methane to methyl bisulfate. The proposed mechanism for Au^{III} also involves initial C–H activation to give a Au^{III}–CH_3 intermediate that is subsequently functionalized, which is very similar to the Hg^{II} cycle. While the catalytic cycle in Fig. 2 is consistent with experimental and computational data in 98% sulfuric acid, it does not readily rationalize products observed in oleum. In contrast to the 98% sulfuric acid conditions, reactions conducted by Sen for methane C–H functionalization with $Hg^{II}(SO_4)$ in oleum at 160 °C resulted in a ~3 : 2 ratio of methanesulfonic acid to methyl bisulfate.[19,20,22] At 90 °C there was only the formation of methanesulfonic acid, indicating this was the kinetic product. As discussed later, methanesulfonic acid can be converted to methyl bisulfate by heating >150 °C in oleum. Because known radical initiators can functionalize methane to produce methanesulfonic acid at low temperatures (90 °C or lower), it was proposed by Sen that with Hg^{II} in oleum methanesulfonic acid is generated by a radical functionalization mechanism,[19,20] which is outlined in Fig. 2 Panel B. Often inferred by the radical functionalization mechanism, but never evaluated, is that in 98% sulfuric acid methanesulfonic acid is first produced as the kinetic product and then methyl bisulfate is subsequently produced as the thermodynamic product.

While lower temperatures have been examined for Hg^{II} reactions, Au^{III} reactions have never been examined at lower temperatures, such as 90 °C, and therefore it is unknown whether methyl bisulfate or methanesulfonic acid is the kinetic product. Also, while reactions with Au^0 have been examined only in 2% weight of SO_3 in sulfuric acid there has previously been no test of reactions of Au_2O_3 with methane in 20% weight of SO_3 in sulfuric acid.

New experiments demonstrating Hg^{II} and Au^{III} reaction selectivity

We decided to perform new experiments because it was unknown what the kinetic product was with Hg^{II} at lower

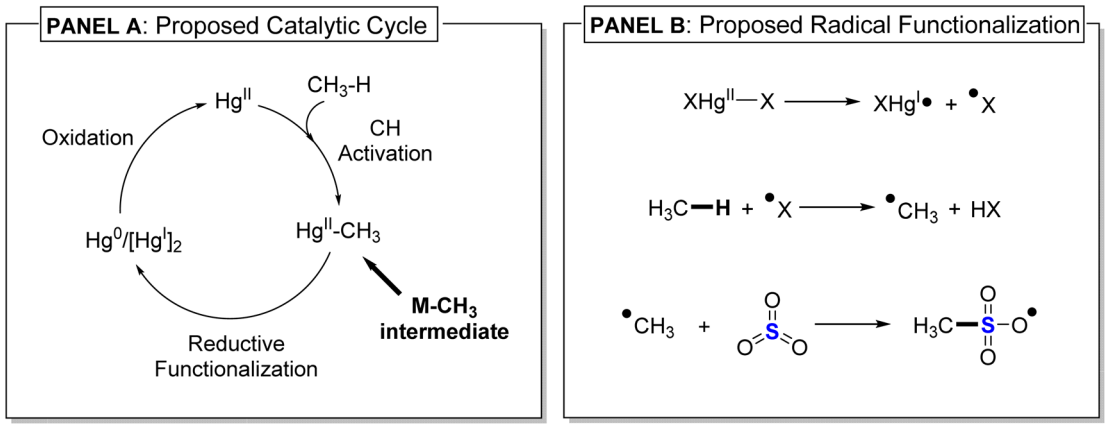

Fig. 2 Panel (A) previously proposed Hg catalytic cycle for forming methyl bisulfate using 98% sulfuric acid. Panel (B) outline of previously proposed mechanism for methanesulfonic acid formation in oleum.

temperatures in 98% sulfuric acid. Also, we decided to complete the low temperature and oleum experiments with Au^{III}. Therefore, to begin our experimental effort, we examined Hg^{II} catalysis with methane in 98% H_2SO_4 and oleum. This was done by preparing a 67 mM solution of $Hg^{II}(SO_4)$ in 98% H_2SO_4 (or D_2SO_4) and in oleum (sulfuric acid, fuming, 20% as free SO_3), in a 10 mL glass insert that was loaded into a stainless-steel pressure reactor pressurized with 500 psig of methane (see the SI for full details). A similar process was completed for Au^{III} reactions using a 66 mM solution generated by dissolving Au_2O_3 in 98% H_2SO_4 (or D_2SO_4) or in oleum.

In 98% H_2SO_4 at 150 °C, both $Hg^{II}(SO_4)$ and Au_2O_3 reactions with methane generated the oxygenation functionalized product methyl bisulfate in near quantitative yields after 3.5 hours (see SI). In the reaction of $Hg(SO_4)$ with methane, the C–H activation/metalation intermediate $(HSO_4)Hg^{II}$–CH_3 (Fig. 3 peak at 1.06 ppm, $^2J_{199Hg,1H} = 264$ Hz) was also observed in ~20% yield. In the Au_2O_3 reaction, no Au–CH_3 intermediate was observed. With observation of the expected products at 150 °C we then examined these 98% H_2SO_4 reactions at a lower temperature of 90 °C. This was done because if the sulfonation functionalization product methanesulfonic acid is generated, it is known to be thermally unstable at high temperatures. For the reaction of $Hg^{II}(SO_4)$ at 90 °C only traces (~1%) of $(HSO_4)Hg^{II}$–CH_3 was observed after three hours. No methanesulfonic acid or methyl bisulfate was observed (Fig. 3, spectrum 3).

The concentration of $(HSO_4)Hg^{II}$–CH_3 doubled when the reaction was run for six hours. For Au^{III} reactions, under the same 98% H_2SO_4 experimental conditions generated only methyl bisulfate in ~2% yield (Fig. 3, spectrum 1). As anticipated, the Hg^{II} reaction is very different in oleum.[19,20] In oleum, the $Hg^{II}(SO_4)$ reaction with methane at 90 °C generated methanesulfonic acid in about 65% yield and $(HSO_4)Hg^{II}$–CH_3 in about 31% yield after one hour. Methyl bisulfate was observed only in trace amounts (Fig. 3, spectrum 4). Regardless of the mechanism for formation of the Hg^{II}–CH_3 bond, observation of this intermediate is consistent with the idea that functionalization selectivity occurs through it (see later computational results). At 150 °C the same reaction generated methanesulfonic acid (359% yield), methyl bisulfate (256% yield), and bis-functionalized product, methanedisulfonic acid, $CH_2(SO_3H)_2$ (102% yield). The intermediate $(HSO_4)Hg^{II}$–CH_3 was generated in about 7% yield.

In contrast to Hg^{II}, methane functionalization reactions in oleum with Au^{III} at 90 °C, generated only methyl bisulfate (41% yield) after 90 minutes (Fig. 3, spectrum 2). No sulfonation functionalization product was observed. Au^{III} also functionalized methane at room temperature in oleum to generate approximately 5% of methyl bisulfate after 2.5 days (see SI). At a temperature of 150 °C, methylenedisulfuric acid, $CH_2(OSO_3H)_2$, started to form due to further functionalization of methyl bisulfate, albeit in traces (~3%) after one hour (see SI).

Overall, these experiments provide compelling evidence that Au^{III} and Hg^{II} have fundamentally different kinetic product selectivity for C–H functionalization. Kinetically, Au^{III} only forms methyl bisulfate while Hg^{II} either forms methanesulfonic acid or methyl bisulfate depending on the sulfuric acid formulation. Consistent with this conclusion, control experiments without Hg^{II} or Au^{III} revealed that methanesulfonic acid is thermally unstable at higher temperatures and converts to methyl bisulfate. At temperatures over 120 °C, in the presence of SO_3, methanesulfonic acid further functionalized to generate methylenedisulfuric acid, and eventually to CO_2 after prolonged heating (see SI). In contrast, methyl bisulfate was found to be thermally stable in oleum in the absence of Hg^{II} or Au^{III} at 150 °C with more than 97% recovery after 60 minutes.

Computational evaluation and selectivity model

With the experimental detection of a $(HSO_4)Hg^{II}$–CH_3 intermediate in both 98% sulfuric acid and oleum conditions, and the new experimental measurements at a lower temperature indicating that methyl bisulfate is the kinetic product at low temperatures, we decided to computationally evaluate Hg^{II} pathways leading from this intermediate to both methanesulfonic acid and methyl bisulfate. The calculations were carried out with M06/def2-TZVPD//M06/def2-SVP using both an implicit solvent model that mimics sulfuric acid and with

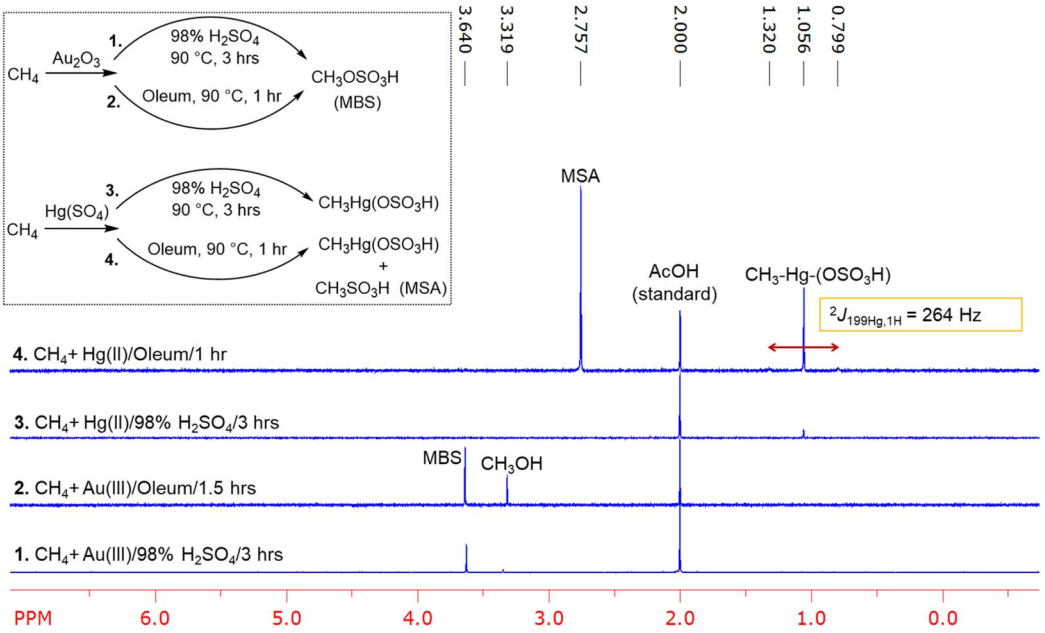

Fig. 3 Overlay of ^{1}H NMR spectra of crude reaction mixtures (reactions shown in the top left corner) of methane functionalization reactions carried out at 90 °C. ^{1}H NMR spectra were recorded after diluting reaction mixtures with D_2O. Spectrum (1): with Au_2O_3 in 98% H_2SO_4 after three hours. Spectrum (2): with Au_2O_3 in oleum after 90 minutes. Spectrum (3): with Hg^{II} in 98% H_2SO_4 after three hours. Spectrum (4): with Hg^{II} in oleum after 60 minutes. MSA = methanesulfonic acid. MBS = methyl bisulfate. AcOH = acetic acid. Note: observed methanol in the ^{1}H NMR spectra are due to the hydrolysis of methyl bisulfate (MBS) by added water.

explicit solvent (see the Computational Methods section for details).

We previously reported the transition structure for bisulfate reacting with $(HSO_4)Hg^{II}$–CH_3 through an S_N2 type reaction mechanism (TS1, Fig. 4).[24] In this transition structure the bisulfate forms the new methyl bisulfate C–O bond with simultaneous cleavage of the Hg–C bond. We examined explicit solvent hydrogen bonding to the bisulfate nucleophile and the weakly coordinating bisulfate anion coordinated to the Hg center. Here, using both a continuum solvent model and an explicit H_2SO_4 solvent the activation enthalpy ($\Delta H^{\ddagger}$) for **TS1** is 35 kcal mol^{-1} and the activation Gibbs energy ($\Delta G^{\ddagger}$) is 33 kcal mol^{-1}, and this is very close to our previous estimate using a slightly different chemical model where $\Delta G^{\ddagger}$ was evaluated to be 34 kcal mol^{-1}.

We also located transition structures for SO_3 reaction with $(HSO_4)Hg^{II}$–CH_3 using explicit and continuum solvent. We identified two different transition structures. A frontside and a backside S_E2 transition structure, and the latter is shown as **TS2** in Fig. 4. The backside S_E2 transition structure was found to be 8 kcal mol^{-1} lower in energy than the frontside S_E2 transition structure. The backside S_E2 transition structure features a linear arrangement of the Hg–C–S atoms. There is explicit hydrogen bonding with the SO_3 portion of the transition structure, which enhances the electrophilicity of SO_3. The formal product of this S_E2 transition structure is an ion pair that with almost no barrier undergoes proton transfer to generate methanesulfonic acid. In this process the Hg center is not formally reduced and remains at Hg^{II}. The backside S_E2 transition structure **TS2** has a $\Delta H^{\ddagger}$ value of 6 kcal mol^{-1} and $\Delta G^{\ddagger}$ value of 21 kcal mol^{-1}, which is 12 kcal mol^{-1} lower in Gibbs energy than the methyl bisulfate forming S_N2 transition structure. The lower energy **TS2** compared to **TS1** is perhaps surprising since in 98% sulfuric acid methyl bisulfate is the major kinetic product. It is useful to note that **TS2** is significantly lower in energy than the Hg–C bond energy in $(HSO_4)Hg$–CH_3, which has a ΔH value of 42 kcal mol^{-1} and ΔG value of 31 kcal mol^{-1}. Therefore, methanesulfonic acid is not generated through a radical, open-shell mechanism stimulated by Hg–C bond homolysis.

As shown in Fig. 4 (middle and bottom panel), an analysis of the intrinsic bond orbitals (IBO)[25] along the intrinsic reaction coordinate (IRC)[26] of **TS1** and **TS2** illustrates the electron flow direction in S_N2 and S_E2 mechanisms. For the S_N2 pathway, the oxygen lone pair in the SO_3H^- abstracts the CH_3^+ and reduces the Hg^{II} to Hg^0. For the S_E2 pathway, electron density from the Hg–CH_3 bond is transferred to the SO_3 to make the new C–S bond and to further oxidize the metal to Hg^{II} species. Natural bond orbital (NBO)[27] charges of Hg (q_{Hg}) and the transferring methyl group (q_{CH3}) along the IRC pathway shows that the S_N2 mechanism requires the reduction of Hg^{II} to Hg^0 whereas for the S_E2 pathway Hg is fully oxidized to Hg^{II} ($q_{Hg} = 1.98e^-$).

With calculations showing that the SO_3 S_E2 reaction pathway *via* **TS2** is significantly lower in energy than the S_N2 reaction pathway, it becomes important to evaluate why in 98% sulfuric acid the kinetic product with Hg^{II} is methyl bisulfate and not methanesulfonic acid. This means that in 98% sulfuric acid, as is well known, there is only a small amount of SO_3 at equilibrium. Therefore, this equilibrium and the energy difference must be determining the overall oxygenation *versus* sulfonation functionalization selectivity. While there are several possible

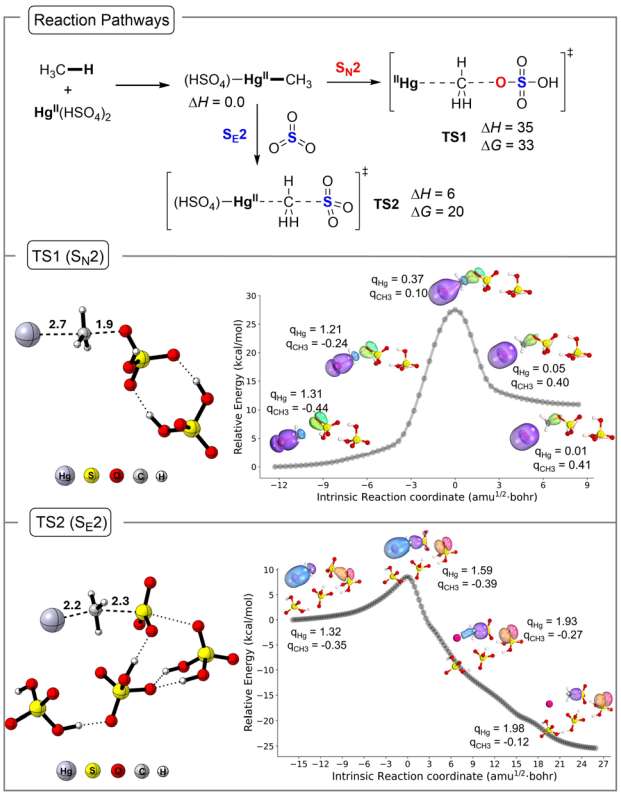

Fig. 4 Top: outline of DFT calculated reaction pathways involving S_N2, and S_E2 transition structures for Hg^{II}–CH_3 functionalization models. Relative enthalpy and Gibbs energy values (in kcal mol^{-1}) were calculated with M06/def2-TZVPD//M06/def2-SVP level of theory. Middle and bottom: geometrical features of **TS1** and **TS2** with IBO and NBO analyses along their IRC pathways.

approaches to calculating the energy of an equilibrium in strong acid, we decided to use a solvent sphere of explicit solvent without any constraints. While this means that the outer edges of the solvent sphere are not treated exactly as bulk solvent, this provides a very reasonable evaluation for explicit solvation effects of H_2SO_4 and its conversion to SO_3 and H_2O within the solvent sphere. Fig. 5 shows the fully optimized H_2SO_4 solvent shell surrounding H_2SO_4 and SO_3/H_2O. These optimized structures were generated by using a cluster growth algorithm where a single H_2SO_4 was sequentially added until

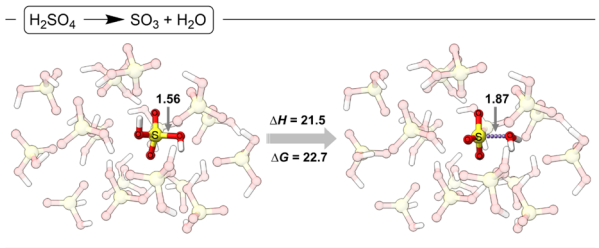

Fig. 5 DFT optimized structures of H_2SO_4 (left-hand side) and SO_3/H_2O (right-hand side) within a solvent sphere of 16 H_2SO_4. Solvent H_2SO_4 are faded for visual clarity. Distances reported in Å and energies (M06/def2-TZVPD//M06/def2-SVP) are in kcal mol^{-1}.

a total of 16 H_2SO_4 were added. At each addition of a sulfuric acid the solute was frozen and 10 different solvent locations were optimized with DFT and only the lowest energy structure was used for a subsequent solvent addition. With these solvent clusters the energy for $H_2SO_4 \rightarrow SO_3 + H_2O$ was calculated to have ΔH of 21.5 kcal mol^{-1} and ΔG of 22.7 kcal mol^{-1}. While it is possible that this energy is overestimated, it is significantly higher than the energy difference between oxygenation and sulfonation pathways (*i.e.* the Gibbs energy difference between **TS1** and **TS2**). In contrast, in oleum, there is essentially no energy required to generate SO_3 and therefore the direct energy difference between **TS1** and **TS2** determines selectivity, with sulfonation being the lowest energy pathway. Importantly, this establishes that an electrophilic S_E2 mechanism can generate methanesulfonic acid.

After establishing that there is an inherent transition state preference for sulfonation functionalization with $(HSO_4)Hg^{II}$–CH_3, we wanted to examine the selectivity for $(HSO_4)_2Au^{III}$–CH_3 functionalization. The experiments showed that only methyl bisulfate is formed as the kinetic product for both 98% sulfuric acid and oleum conditions. Therefore, we hypothesized that the Au^{III} inverts the relative energies of S_N2 and S_E2 transition states. Previous calculations by Goddard and Periana showed that Au^{III} is capable of electrophilic substitution with methane to generate a Au^{III}–CH_3 intermediate that can be functionalized.[23] Goddard also previously proposed that functionalization occurs through the overall anionic $[(HSO_4)_3Au^{III}$–$CH_3]^-$ intermediate.[23] Therefore, we examined functionalization using this anionic model with an added explicit H_2SO_4 solvent as well as the neutral complex $(H_2SO_4)(HSO_4)_2Au^{III}$–$CH_3$. We also considered the possibility that functionalization occurs though Au^{III}–Au^{III} bridged species, but these barriers were similar to the mononuclear barriers. It is also important to note that as the Au-methane reaction progresses there is formation of Au^I and that this species can also react with methane to generate a Au^I–CH_3 intermediate. However, if significant C–H activation reactivity occurs between Au^I and methane to generate a Au^I–CH_3 intermediate, our calculations suggest that there would be rapid methyl transfer to Au^{III} for the functionalization. As an example, ligand exchange for $Au^{III}(HSO_4)_3$ + Au^I–CH_3 → $(HSO_4)_2Au^{III}$–CH_3 + $Au^I(HSO_4)$ is exergonic by 31 kcal mol^{-1}.

Fig. 6 and 7 outline the functionalization results for $(H_2SO_4)(HSO_4)_2Au^{III}$–$CH_3$ and $[(HSO_4)_3Au^{III}$–$CH_3]^-$. Not shown, but as expected, the Au^{III}–CH_3 bond in $(HSO_4)_2Au^{III}$–CH_3 is stronger than the Hg^{II}–CH_3 bond in $(HSO_4)Hg^{II}$–CH_3 ($\Delta H > 50$ kcal mol^{-1} for both neutral and anionic models) therefore, homolysis-driven functionalization is very unlikely. For the neutral system the transition structure for methyl bisulfate formation by a S_N2 type reaction mechanism (**TS3**, Fig. 6) has a $\Delta H^{\ddagger}$ value of 26 kcal mol^{-1} and $\Delta G^{\ddagger}$ value of 26 kcal mol^{-1}. For the anionic system, (**TS3_anionic**, Fig. 7) has a $\Delta H^{\ddagger}$ value of 14 kcal mol^{-1} and $\Delta G^{\ddagger}$ value of 15 kcal mol^{-1}. The neutral and anionic transition structure **TS3** is similar to the structure previously reported by Goddard and Periana and very similar to the Hg transition structure where it features a linear arrangement of the bisulfate oxygen, the methyl group carbon, and the Au center.

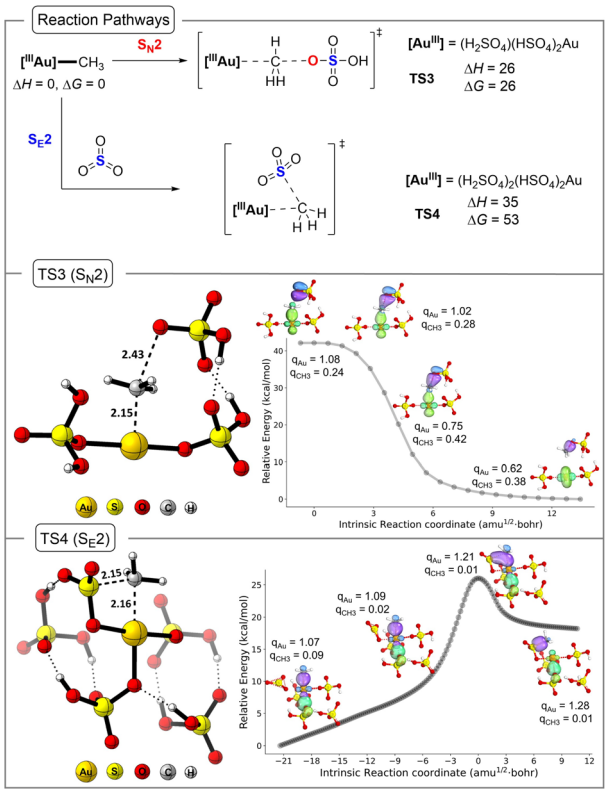

Fig. 6 Top: outline of DFT calculated S_N2 and S_E2 transition structures for neutral Au–CH_3 functionalization models. Enthalpies and Gibbs energies reported refer to M06/def2-TZVPD//M06/def2-SVP (kcal mol^{-1}). Middle and bottom: geometrical features of **TS3** and **TS4** with IBO and NBO analyses along their IRC pathways.

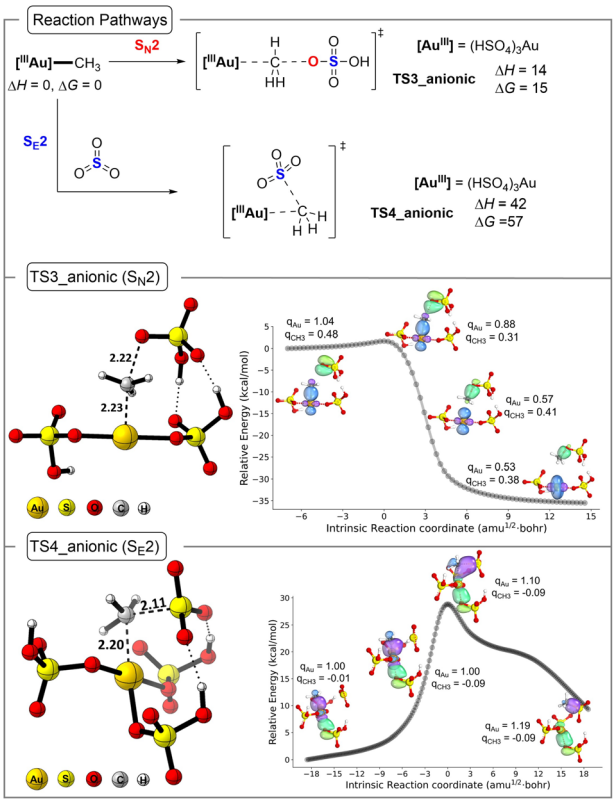

Fig. 7 Top: outline of DFT calculated S_N2 and S_E2 transition structures for anionic Au–CH_3 functionalization models. Enthalpies and Gibbs energies reported refer to M06/def2-TZVPD//M06/def2-SVP (kcal mol^{-1}). Middle and bottom: Geometrical features of **TS3_anionic** and **TS4_anionic** with IBO and NBO analyses along their IRC pathways.

Fig. 6 and 7 also give the transition structure energies for functionalization of the Au^{III}–CH_3 bond with SO_3. For the neutral system, this involves a frontside SO_3 S_E2 type transition structure (see 3D structure; **TS4**). Despite significant searching, we were unable to locate the backside S_E2 transition structure. For the neutral system, the $\Delta H^{\ddagger}$ value for **TS4** is 35 kcal mol^{-1}, and this is 9 kcal mol^{-1} higher in energy than **TS3**. For the anionic system, the $\Delta H^{\ddagger}$ value for **TS4_anionic** is 42 kcal mol^{-1}, and this is 28 kcal mol^{-1} higher in energy than **TS3_anionic**. Analysis of the Gibbs energies also shows the same preference and lower energy pathway involving **TS3**.

IBO analysis along the IRC path presented in Fig. 6 and 7 (middle and bottom panel) establishes the characteristics of S_N2 and S_E2 mechanisms for Au, which are similar to that observed in Hg reactions. The NBO charge analysis of the **TS3** and **TS4** in both neutral and anionic states establishes the reluctance of Au to be further oxidized during the S_E2 mechanism where the methyl anion is transferred. Overall, this confirms that the effective electrophilicity of Au^{III} compared to the less electronegative Hg^{II} inverts the reaction pathway preference. Specifically, for Au^{III} with the bisulfate nucleophile (neutral pathway), the S_N2 transition structure is about 9 kcal mol^{-1} lower in enthalpy than the Hg^{II} transition structure. This is readily rationalized by Au^{III} being a much better leaving group with a larger Au^{III} to Au^{I} reduction potential compared to the Hg^{II} to Hg^{0} reduction potential. The selectivity is also influenced by a S_E2 transition structure where the Au^{III} version is destabilized relative to the Hg^{II} version. The neutral **TS4** is nearly 30 kcal mol^{-1} higher in energy than **TS2**.

Experiments that support computational-based selectivity model

With calculations indicating that a closed-shell reaction mechanism provides adequate explanation for kinetic product selectivity with Hg^{II} and Au^{III}, and that there is no need to invoke a radical functionalization mechanism, we decided to test this prediction experimentally. Therefore, additional methane reactions with Hg^{II} and Au^{III} were carried out in both 98% H_2SO_4 and oleum under an oxygen atmosphere. Oxygen is a well-established radical scavenger for alkane functionalization reactions and is known to suppress radical pathways.[20,28] Reactions conducted in the presence of 14.7 psi (1 atm) of O_2 and 485.5 psi CH_4 showed no change in product selectivity, suggesting that no significant concentration of metal and carbon radicals are involved in the functionalization reactions.

Also, the implication of the calculated pathways is that if Hg^{II}–CH_3 and Au^{III}–CH_3 intermediates are synthesized and then subjected to sulfuric acid solvent environments there will be

predictable product selectivity. Therefore, we carried out several reactions with different solvent environments and where Hg^{II}–CH_3 was first synthesized and then subjected several functionalization reaction conditions, including with Au^{III} where we hypothesized that Hg-to-Au methyl group transfer would be very fast.

The first reaction carried out was in a 1:1 mixture of 98% H_2SO_4 to oleum (containing 20 weight% free SO_3), resulting in an effective free SO_3 concentration of approximately 6 weight%. Methane functionalization using $Hg^{II}(SO_4)$ in this acid solvent mixture generated methanesulfonic acid as the primary product, with a yield of ~21% when the reaction was conducted at 90 °C for 3 hours (see the SI). A similar product distribution was observed at 110 °C after 1 hour, where methanesulfonic acid remained the dominant product (~27% yield after 1 hour), and only trace amounts of methyl bisulfate were detected (see the SI). These results suggest that methanesulfonic acid is the favored initial product in the presence of free SO_3, despite the abundance of bisulfate anions in the reaction medium that could otherwise facilitate the formation of the alternative methyl bisulfate product, and this is consistent with the calculated reaction selectivity. No methane functionalization experiments were conducted with Au_2O_3 in this medium because as stated above Au^{III} only produced methyl bisulfate as the initial product in both neat 98% H_2SO_4 and oleum (20 weight% SO_3 in H_2SO_4), regardless of temperature.

To further understand the difference in solvent dependent product selectivity with Hg^{II} and Au^{III}, we performed methyl transfer reactions between separately synthesized $(HSO_4)Hg^{II}$–CH_3 and Au^{III} in 98% H_2SO_4, in oleum, and in a mixture of 98% H_2SO_4 and oleum (Scheme 1). The intermediate $(HSO_4)Hg^{II}$–CH_3 was prepared in 98% H_2SO_4 following the procedure described above by reacting methane with $HgSO_4$ at 110 °C for five hours (reaction *a* in Scheme 1 and Fig. 8, spectrum 1). Then in a Schlenk bomb flask at 0 °C, ~0.01 mmol of the $(HSO_4)Hg^{II}$–CH_3 made through reaction *a* was mixed with oleum, making a 3 : 1 ratio of oleum and 98% H_2SO_4 (reaction *b* in Scheme 1). This reaction mixture was then gradually warmed to room temperature and stirred at room temperature for two additional hours. ^1H NMR analysis of the resultant reaction mixture showed only traces of methanesulfonic acid, indicating a somewhat slow reaction of $(HSO_4)Hg^{II}$–CH_3 with SO_3 (Fig. 8, spectrum 2). Similarly, reaction of ~0.01 mmol of $(HSO_4)Hg^{II}$–CH_3 with 2 equivalents of Au^{III} solution prepared in 98% H_2SO_4 (reaction *c* in Scheme 1) resulted in quantitative conversion of $(HSO_4)Hg^{II}$–CH_3 to methyl bisulfate (Fig. 8, spectrum 3).

We also investigated competitive methyl group functionalization in the presence of both Au^{III} and SO_3, where SO_3 was present in ~67-fold excess relative to Au^{III} (reaction *d* in Scheme 1). In the first competition reaction a ~0.01 mmol solution of $(HSO_4)Hg^{II}$–CH_3 prepared in 98% H_2SO_4 was added to oleum (see SI) at 0 °C. After stirring the mixture for 30 minutes, ~2 equivalents of Au^{III} (relative to $(HSO_4)Hg^{II}$–CH_3), prepared in 98% H_2SO_4, were introduced to achieve a final molar ratio of $[Au^{III}]:[SO_3] \approx 0.02{:}1.34$. The reaction mixture warmed to room temperature and then stirred for an additional 90 minutes at room temperature (reaction *d* in Scheme 1). ^1H NMR analysis of the resultant reaction mixture indicated generation of only the oxygenation product methyl bisulfate in quantitative yields with negligible amounts of the sulfonation product methanesulfonic acid (Fig. 8, spectrum 4). The formation of only methyl bisulfate can be interpreted by relatively fast and irreversible methyl group transfer from Hg to Au followed by functionalization of a Au^{III}–CH_3 methyl species. Similarly, a second competition reaction in oleum where there is a large excess of SO_3 compared to Au^{III} was carried out. This involved the initial reaction of Hg^{II} with methane in oleum at 90 °C to generate both $(HSO_4)Hg^{II}$–CH_3 and methanesulfonic acid (reaction *e* in Scheme 1 and Fig. 8, spectrum 5, also see the SI). Then at room temperature the resultant oleum reaction mixture was treated with ~2 equivalents of Au^{III}, with respect to the concentration of $(HSO_4)Hg^{II}$–CH_3 (reaction *f* in Scheme 1). This second competition reaction also generated exclusively methyl bisulfate, and the concentration of methanesulfonic acid was nearly unchanged, suggesting that methanesulfonic acid was stable under these specific reaction conditions (Fig. 8, spectrum 6). Again, this reaction suggests that $(HSO_4)Hg^{II}$–CH_3 preferentially reacts with Au^{III} followed by functionalization to generate methyl bisulfate. Importantly, control experiments showed that methanesulfonic acid is stable in the presence of Au^{III} in oleum under these reaction conditions used. As another confirmation of the Au^{III} functionalization selectivity, we treated tetramethyltin with Au^{III} both in 98% H_2SO_4 and oleum. Similar to the reaction between $(HSO_4)Hg^{II}$–CH_3 and Au^{III}, we observed methyl bisulfate in quantitative yields with respect to added Au^{III} both in 98% H_2SO_4 and oleum. In oleum, we also observed methanesulfonic acid, due to the functionalization of methyltin species. Control experiments in oleum with only tetramethyltin generated methanesulfonic acid along with methane in the absence of any added Au^{III}. In 98% H_2SO_4, tetramethyltin did not undergo any type of functionalization in the absence of Au^{III} other than protonation of methyl group to generate methane under same reaction conditions. See SI for more details. These

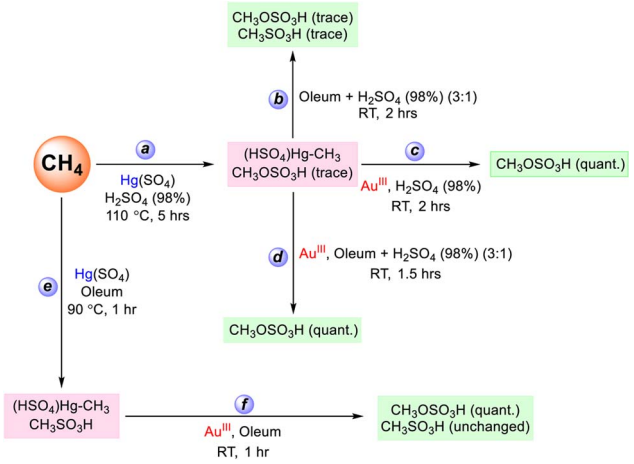

Scheme 1 Outline of methyl transfer reactions used to evaluate metal and solvent dependent product selectivity. See Fig. 8 for the corresponding ^1H NMR spectra.

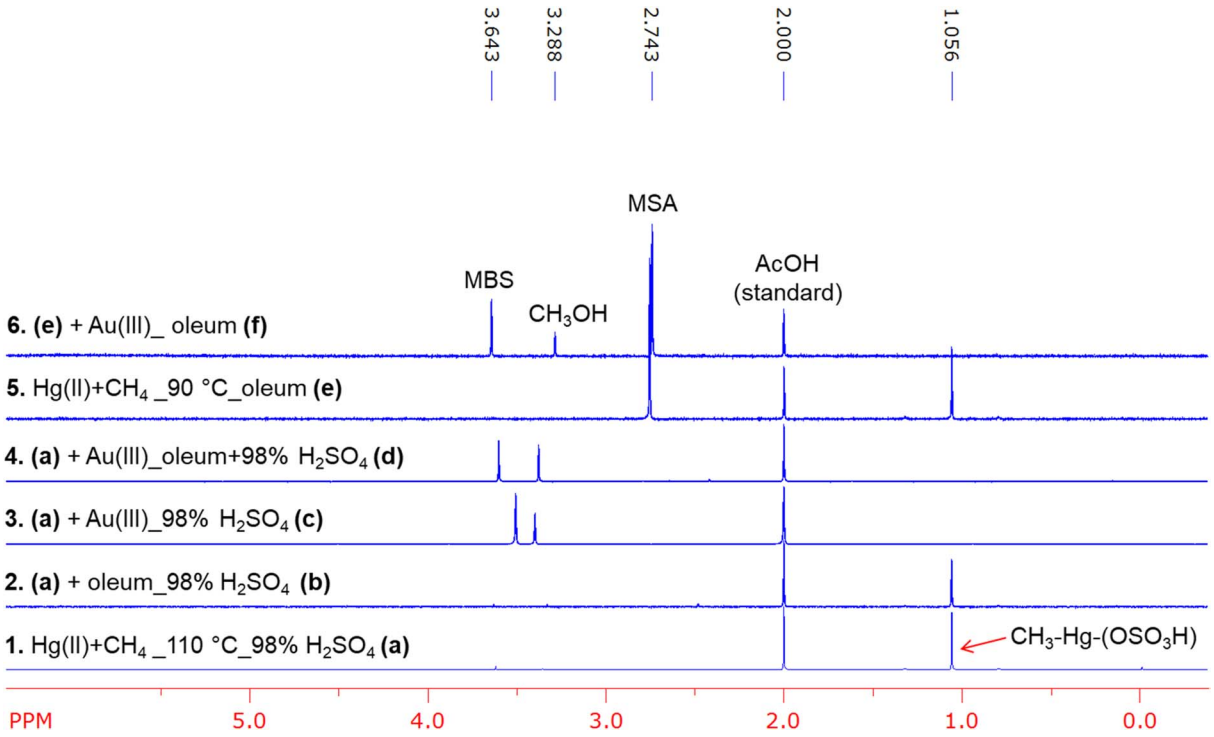

Fig. 8 Overlay of ^{1}H NMR spectra of reaction mixtures (**a**–**f**) outlined in Scheme 1. Spectrum (1): reaction of methane with $Hg(SO_4)$ in 98% H_2SO_4 carried out at 110 °C for 5 hours (**a**). Spectrum (2): reaction of $(HSO_4)Hg–CH_3$ from **a** with oleum at room temperature for two hours (**b**). Spectrum (3): reaction of $(HSO_4)Hg–CH_3$ from **a** with Au^{III} in 98% H_2SO_4 run for 1.5 hours at room temperature (**c**). Spectrum (4): reaction of $(HSO_4)Hg–CH_3$ from c with Au^{III} in a 1 : 3 mixture 98% H_2SO_4 and oleum run for 1.5 hours at room temperature (**d**). Spectrum (5): reaction of methane and $HgSO_4$ carried out in oleum at 90 °C for one hour (**e**). Spectrum (6): reaction of products from **e** with Au^{III} prepared in oleum (**f**). Note: Observed methanol in the ^{1}H NMR spectra are due to the hydrolysis of methyl bisulfate (MBS) by added water. MSA = methanesulfonic acid.

competition experiments strongly argue against involvement of any methyl radical species as they would be quickly trapped by excess SO_3 to generate methanesulfonic acid. Instead these reactions support a closed-shell, electrophilic methyl-transfer/heterolytic functionalization sequence.

Conclusions

New experiments and calculations have revealed that the kinetic products generated for methane C–H functionalization with Hg^{II} and Au^{III} catalysis in 98% sulfuric acid and oleum occur through a non-radical, closed-shell mechanism. For Hg^{II}, oxygenation to give methyl bisulfate occurs in 98% sulfuric acid while sulfonation to give methanesulfonic acid occurs in oleum. In contrast, Au^{III} only induces oxygenation functionalization of methane in both 98% sulfuric acid and oleum. Experiments and DFT calculations indicate that oxygenation *versus* sulfonation selectivity occurs from the Hg^{II}–CH_3 and Au^{III}–CH_3 intermediates. This selectivity model involves the competition between a bisulfate S_N2 type mechanism (oxygenation pathway) and a S_E2 mechanism (sulfonation pathway) with SO_3. For the Hg^{II}–CH_3 intermediate the barrier for the S_E2 transition structure is significantly lower than the barrier for the S_N2 transition structure. This means that the sulfuric acid to SO_3/H_2O equilibrium controls S_N2 *versus* S_E2 selectivity. In 98% sulfuric acid this equilibrium is highly unfavorable, which was estimated using a sphere of explicit solvent, and therefore the S_N2 pathway is lower in energy. In contrast, in oleum with free SO_3 the S_E2 pathway is lower in energy. For Au^{III}–CH_3, the selectivity of transition structures is reversed and the S_N2 transition structure is lower in energy than the S_E2 transition structure, and this change correlates with the higher Au^{III} to Au^{I} reduction potential compared to Hg^{II} to Hg^0 reduction potential.

Computational methods

Calculations were mainly performed in Gaussian 16.[29] For geometry optimizations M06 (ref. 30)/def2-SVP was used. The use of larger basis sets, such as def2-TZVPD, to optimize structures showed nearly identical geometries. Therefore, we executed single point energies with the def2-TZVPD and the reported energies are M06/def2-TZVPD//M06/def2-SVP. Additional single-point energies with alternative density functionals and basis sets as a comparison were evaluated using ORCA[31] and reported in the SI. All structures reported were confirmed as a minima or a saddle point through vibrational frequency calculations, which were also used to generate thermochemical corrections at 298 K and 1 atm. All geometries were optimized with a PCM[32] solvent model with parameters that mimic 98% sulfuric acid (EPS = 98.0, radius = 2.205). While the dielectric of sulfuric acid decreases at high temperatures the exact value is unknown. Test calculations that use an EPS keyword value

below 98.0 showed no significant difference for calculated structures and energies. Importantly, all calculations included at least one explicit H_2SO_4 solvent molecule. Each structure reported is the lowest energy of a set of configurations generated through manual searching as well as using CREST/x-TB.[33,34] IBO calculations were performed using the IBOView software.[25] Natural charges were obtained from NBO analyses as implemented in Gaussian 16. For the explicit solvent evaluation of the $H_2SO_4 \rightarrow SO_3 + H_2O$ energy, 16 H_2SO_4 molecules that were added to each side of the reaction equation. Each explicit solvent was sequentially added using CREST's QCG tool.[35] For each sequential addition, the 10 lowest energy xTB structures were optimized with DFT and then only the lowest energy DFT structure was carried onto adding additional sulfuric acid molecules.

Author contributions

D. H. Ess designed the experimental and computational studies, analyzed data, and wrote the manuscript. A. Koppaka designed experimental studies, executed experimental studies, interpreted data, and wrote the manuscript. C. Cullimore carried out calculations, interpreted data, and wrote part of the manuscript. J. Joy and A. Kraus carried out calculations. R. A. Periana analyzed and interpreted data.

Conflicts of interest

There are no conflicts to declare.

Data availability

Data supporting this work is part of the supporting information (SI). Supplementary information: additional experimental details, *xyz* coordinates, and absolute energy of optimized DFT structures. See DOI: https://doi.org/10.1039/d6sc01628f.

Acknowledgements

We thank Brigham Young University and the Office of Research computing, especially the Fulton Supercomputing Lab. This work was fully supported by the U.S. Department of Energy, Office of Science, Basic Energy Sciences, Catalysis Science Program, under Award # DE-SC0018329.

Notes and references

1 N. J. Gunsalus, A. Koppaka, S. H. Park, S. M. Bischof, B. G. Hashiguchi and R. A. Periana, Homogeneous Functionalization of Methane, *Chem. Rev.*, 2017, **117**, 8521–8573.
2 R. H. Crabtree, Alkane C–H activation and functionalization with homogeneous transition metal catalysts: a century of progress a new millennium in prospect, *J. Chem. Soc., Dalton Trans.*, 2001, 2437–2450.
3 R. H. Crabtree, The organometallic chemistry of alkanes, *Chem. Rev.*, 1985, **85**, 245–269.
4 R. H. Crabtree, Aspects of Methane Chemistry, *Chem. Rev.*, 1995, **95**, 987–1007.
5 S. M. Bischof, B. G. Hashiguchi, M. M. Konnick and R. A. Periana, Designing Molecular Catalysts for Selective CH Functionalization. In *Topics in Organometallic Chemistry: Inventing Reactions*, ed. Gooßen, L. J., Springer-Verlag, Berlin, 2013, vol. 44, pp. 195–232.
6 B. G. Hashiguchi, C. H. Hövelmann, S. M. Bischof, K. S. Lokare, C. H. Leung and R. A. Periana, in. *Methane-to-Methanol Conversion*. Encyclopedia of Inorganic and Bioinorganic Chemistry, 2011, DOI: 10.1002/9781119951438.eibc0456.
7 B. L. Conley, W. J. Tenn III, K. J. H. Young, S. K. Ganesh, S. K. Meier, V. R. Ziatdinov, O. Mironov, J. Oxgaard, J. Gonzales, W. A. Goddard III and R. A. Periana, Design and study of homogeneous catalysts for the selective, low temperature oxidation of hydrocarbons, *J. Mol. Catal. A: Chem.*, 2006, **251**, 8–23.
8 T. B. Gunnoe, In *Alkane C-H Activation by Single-Site Metal Catalysts*, ed. Perez, P. J., Springer, Dordrecht, 2012, Vol. 38, pp. 1–17.
9 B. G. Hashiguchi, S. M. Bischof, M. M. Konnick and R. A. Periana, Designing Catalysts for Functionalization of Unactivated C-H Bonds Based on the CH Activation Reaction, *Acc. Chem. Res.*, 2012, **45**, 885–898.
10 A. E. Shilov, in. *Activation of Saturated Hydrocarbons by Transition Metal Complexes*, D. Reidel Publishing Co., Dordrecht, The Netherlands, 1984.
11 A. E. Shilov and A. A. Shteinman, Activation of saturated hydrocarbons by metal complexes in solution, *Coord. Chem. Rev.*, 1977, **24**, 97–143.
12 J. A. Labinger and J. E. Bercaw, Understanding and exploiting C–H bond activation, *Nature*, 2002, **417**, 507–514.
13 G. S. Chen, J. A. Labinger and J. E. Bercaw, The role of alkane coordination in C–H bond cleavage at a Pt(II) center, *Proc. Natl. Acad. Sci. U. S. A.*, 2007, **104**, 6915–6920.
14 A. E. Shilov and G. B. Shul'pin, in. *Activation and Catalytic Reactions of Saturated Hydrocarbons in the Presence of Metal Complexes*, Kluwer Academic, Dordrecht, The Netherlands, 2000.
15 B. G. Hashiguchi, M. M. Konnick, S. M. Bischof, S. J. Gustafson, D. Devarajan, N. Gunsalus, D. H. Ess and R. A. Periana, Main-Group Compounds Selectively Oxidize Mixtures of Methane, Ethane, and Propane to Alcohol Esters, *Science*, 2014, **343**, 1232–1237.
16 S. J. Gustafons, J. T. Fuller III, D. Devarajan, J. Snyder, R. A. Periana, B. G. Hasiguchi, M. M. Konnick and D. H. Ess, Contrasting Mechanisms and Reactivity of Tl(III), Hg(II), and Co(III) for Alkane C-H Functionalization, *Organometallics*, 2015, **34**, 5485–5495.
17 A. Koppaka, S. H. Park, B. G. Hashiguchi, N. J. Gunsalus, C. R. King, M. M. Konnick, D. H. Ess and R. A. Periana, Selective C-H Functionalization of Methane and Ethane by a Molecular Sb(V) Complex, *Angew. Chem., Int. Ed.*, 2019, **58**, 2241–2245.
18 S. Mukhopadhyay and A. T. Bell, Direct Sulfonation of Methane to Methanesulfonic Acid by Sulfur Trioxide

Catalyzed by Cerium(IV) Sulfate in the Presence of Molecular Oxygen, *Adv. Synth. Catal.*, 2004, **346**, 913–916.

19 A. Sen, M. A. Benvenuto, M. Lin, A. C. Hutson and N. Basickes, Activation of Methane and Ethane and Their Selective Oxidation to the Alcohols in Protic Media, *J. Am. Chem. Soc.*, 1994, **116**, 998–1003.

20 N. Basickes, T. E. Hogan and A. Sen, Radical-Initiated Functionalization of Methane and Ethane in Fuming Sulfuric Acid, *J. Am. Chem. Soc.*, 1996, **118**, 13111–13112.

21 R. A. Periana, D. J. Taube, E. R. Evitt, D. G. Löffler, P. R. Wentrcek, G. Voss and T. Masuda, A mercury-catalyzed, high-yield system for the oxidation of methane to methanol, *Science*, 1993, **259**, 340–343.

22 A. Sen, Catalytic Functionalization of Carbon−Hydrogen and Carbon−Carbon Bonds in Protic Media, *Acc. Chem. Res.*, 1998, **31**, 550–557.

23 C. J. Jones, D. Taube, V. R. Ziatdinov, R. A. Periana, R. J. Nielsen, J. Oxgaard and W. A. Goddard III, Selective Oxidation of Methane to Methanol, Catalyzed with C-H Activation, by Homogeneous, Cationic Gold, *Angew. Chem., Int. Ed.*, 2004, **43**, 4626–4629.

24 J. T. Fuller III, S. Butler, D. Devarajan, A. Jacobs, B. G. Hashiguchi, M. M. Konnick, W. A. Goddard III, J. Gonzales, R. A. Periana and D. H. Ess, Catalytic Mechanism and Efficiency of Methane Oxidation by Hg(II) in Sulfuric Acid and Comparison to Radical Initiated Conditions, *ACS Catal.*, 2016, **6**, 4312–4322.

25 G. Knizia, Intrinsic Atomic Orbitals: An Unbiased Bridge between Quantum Theory and Chemical Concepts, *J. Chem. Theory Comput.*, 2013, **9**, 4834–4843.

26 K. Fukui, The path of chemical reactions - the IRC approach, *Acc. Chem. Res.*, 1981, **14**, 363–368.

27 A. E. Reed, R. B. Weinstock and F. Weinhold, Natural population analysis, *J. Chem. Phys.*, 1985, **83**, 735–746.

28 I. P. Stolarov, M. N. Vargaftik, D. I. Shishkin and I. I. Moiseev, Oxidation of ethane and propane with cobalt(II) catalyst: unexpected formation of 1,2-diol esters and C–C bond cleavage, *J. Chem. Soc. Chem. Commun.*, 1991, 938–939.

29 M. J. Frisch, G. W. Trucks, H. B. Schlegel, G. E. Scuseria, M. A. Robb, J. R. Cheeseman, G. Scalmani, V. Barone, G. A. Petersson, H. Nakatsuji, X. Li, M. Caricato, A. V. Marenich, J. Bloino, B. G. Janesko , R. Gomperts, B. Mennucci, H. P. Hratchian, J. V. Ortiz, A. F. Izmaylov, J. L. Sonnenberg, D. Williams-Young, F. Ding, F. Lipparini, F. Egidi, J. Goings, B. Peng, A. Petrone, T. Henderson, D. Ranasinghe, V. G. Zakrzewski, J. Gao, N. Rega, G. Zheng, W. Liang, M. Hada, M. Ehara, K. Toyota, R. Fukuda, J. Hasegawa, M. Ishida, T. Nakajima, Y. Honda, O. Kitao, H. Nakai, T. Vreven, K. Throssell, J. A. Montgomery Jr, J. E. Peralta, F. Ogliaro, M. J. Bearpark, J. J. Heyd, E. N. Brothers, K. N. Kudin, V. N. Staroverov, T. A. Keith, R. Kobayashi, J. Normand, K. Raghavachari, A. P. Rendell, J. C. Burant, S. S. Iyengar, J. Tomasi, M. Cossi, J. M. Millam, M. Klene, C. Adamo, R. Cammi, J. W. Ochterski, R. L. Martin, K. Morokuma, O. Farkas, J. B. Foresman and D. J. Fox, *Gaussian 16, Revision B.01*, Gaussian, Inc., Wallingford, CT, 2019.

30 C. J. Cramer and D. G. Truhlar, Density functional theory for transition metals and transition metal chemistry, *Phys. Chem. Chem. Phys.*, 2009, **11**, 10757–10816.

31 F. Neese, The ORCA program system, *WIREs Comput. Mol. Sci.*, 2012, **2**, 73–78.

32 J. Tomasi, B. Mennucci and R. Cammi, Quantum mechanical continuum solvation models, *Chem. Rev.*, 2005, **105**, 2999–3093.

33 P. Pracht, F. Bohle and S. Grimme, Automated exploration of the low-energy chemical space with fast quantum chemical methods, *Phys. Chem. Chem. Phys.*, 2020, **22**, 7169–7192.

34 S. Spicher and S. Grimme, Robust Atomistic Modeling of Materials, Organometallic, and Biochemical Systems, *Angew. Chem., Int. Ed.*, 2020, **59**, 15665–15673.

35 S. Spicher, C. Plett, P. Pracht, A. Hansen and S. Grimme, Automated Molecular Cluster Growing for Explicit Solvation by Efficient Force Field and Tight Binding Methods, *J. Chem. Theory Comput.*, 2022, **18**(5), 3174–3189.